Smart Sensor for fault detection in Induction Motors Based on the Combined Analysis of Stray Flux and Current signals

Israel Zamudio-Ramírez, Roque A. Osornio-Rios, *Member, IEEE,* and Jose Alfonso Antonino-Daviu, *Senior Member, IEEE.*

***Abstract*— The most recent trend in the electric motor condition monitoring area relies on combining the information obtained from different machine quantities in order to reach a more reliable conclusion about the motor's health. This knowledge is of critical importance nowadays, especially in industrial applications in which unexpected outages can lead to severe repercussions. This paper presents a new intelligent sensor that combines, in a single unit, the information obtained from the analysis of stray fluxes (both axial and radial) and currents by means of a feed-forward neural network (FFNN) for classification purposes. Unlike other solutions, the sensor is based on the application of advanced signal processing tools that are adapted to the online analysis of these quantities under transient from a single processing unit (smart sensor). The combination of these new tools with the classical steady-state analysis of such quantities enables to obtain a more reliable conclusion on the motor health. The experiments included in the paper demonstrate the reliability provided by the sensor, which is being prepared to incorporate a third input based on infrared data.**

***Index Terms*— fault diagnosis, induction motor, stray flux, transient analysis, time-frequency transforms**

I. Introduction

THE electric motor predictive maintenance area is living a renewed dynamism over recent years. The vast participation of these machines in a wide variety of industrial processes together with their prominent role in modern applications that are the core of future societies (e.g. electric vehicles) convert them into crucial assets, so that the determination of their health is of primordial importance [1]. Note that the presence of defects and anomalies in these machines has not only repercussions in terms of risk for their integrity (with potential motor outages and production downtimes), but also affects the efficiency and performance of the machine itself. In this regard, recent works have proven that, in the event that certain defects are present, the motor efficiency is seriously compromised so that it may operate during long intervals below its rated features [2], [3].

Due to all these facts, there has been an intensive effort toward the search of reliable diagnosis systems, which include methods able to determine the motor's health with high reliability and accuracy. In this context, several techniques have been proposed as a basis of those systems: analysis of vibration signals [4], [5], infrared data [6], [7], stray fluxes [8], partial discharges [9], [10], acoustic signals [11], among others. Each technique has provided satisfactory results for the diagnosis of certain faults or anomalies. However, it is a fact that no single technique has been proven to be reliable enough to diagnose all the possible failures that can appear in the electric motor. In other words, each technique is valid for detecting certain faults but not for others. And, even for those failures for which a technique works well, there may be cases in which the application of the method may be unsuitable or provide false indications [12].

This situation explains the current trend, which is also followed by several manufacturers, that is oriented toward the construction of modern diagnosis systems that are not based on the analysis of a single quantity, but that rely on the combined analysis of different machine quantities. The idea is to merge the information obtained from the application of several techniques in order to reach a more robust diagnosis of the machine condition. Some recent works have proposed this type of collaborative systems [13]. Nonetheless, most collaborative diagnostic systems process information offline. Furthermore, an additional research effort is still needed to find a combined system that is reliable enough to reach an accurate diagnosis conclusion for the detection of a certain range of faults, avoiding false indications of the current methods and, at the same time, able to be used under any

This work was derived from a project supported by the Beca Leonardo a Investigadores y Creadores Culturales 2019 of Fundación BBVA (ref: IN[19]_ING_ING_0083). BBVA Foundation is not responsible of the opinions, comments or contents included in the project or the results derived from it. These are exclusive responsibility of the authors.

I. Zamudio-Ramirez is with the CA Mecatronica, Facultad de Ingenieria, Campus San Juan del Rio, Universidad Autónoma de Querétaro, San Juan del Río, 76807 Querétaro, MEXICO, and with the Department of Electrical Engineering, Universitat Politècnica de València, Camino de Vera s/n, 46022, Valencia, SPAIN (e-mail: iszara@doctor.upv.es).

R. A. Osornio-Rios is with the CA Mecatronica, Facultad de Ingenieria, Campus San Juan del Rio, Universidad Autónoma de Querétaro, San Juan del Río, 76807 Querétaro, MEXICO (e-mail: raosornio@hspdigital.org).

J. Antonino-Daviu is with the Instituto Tecnologico de la Energia, Universitat Politècnica de València, Camino de Vera s/n, 46022, Valencia, SPAIN (e-mail: joanda@die.upv.es).

possible operation regime of the machine (including transients).

This paper presents a new collaborative system that combines, in a single unit, the application of the most recent technologies relying on stray flux and current analysis. The proposed system, which constitutes an extension of the one already introduced in [14], takes advantage of the spectacular advance in the technology of smart sensors, which provide not only measurement capabilities but also onsite processing features making it a low-cost alternative able to be installed anywhere on the frame of the machine, compact, and non-invasive [15], [16]. Regarding the measurement of stray flux data, the developed smart system uses an innovative triaxial sensor that can capture the stray flux in different directions and therefore, enabling the detection of the different components (radial/axial) modified by the considered failures. The processing unit relies on the combined application of classical methods (relying on stationary analysis) with modern technologies (based on time-frequency analysis of transient features), whose validity has been proven in previous works [10], [17]. Moreover, fault severity indicators based on the evaluation of the energy density in particular time-frequency regions are proposed. These fault indicators are the inputs of a feed-forward neural network (FFNN), which allows for an automated final diagnosis. The sensor is applied to the detection of rotor damages and eccentricities/misalignments. The results prove the potential of the proposed intelligent solution.

II. Combined Stray Flux & Current Analysis

The proposed diagnosis system relies on the combined analysis of stray flux and current data. In this way, the sensor performs the acquisition of these data both under steady-state and under starting, and processes each quantity with suitable signal processing tools. A time-frequency tool, the optimized Short Time Fourier Transform (STFT) is applied to the stray flux and current data captured under starting and during steady-state in order to extract information from transient states as well as from stationary states. Therefore, the developed system takes advantage of the important benefits of transient analysis, which has proven to be very effective for the diagnosis, avoiding occasional false indications obtained with the classical methods. In this regard, in the case of currents, the analysis of the starting current, enables to avoid false positive/negative indications caused by constructive characteristics of the machine or operation conditions [17]. On the other hand, flux-based analysis under starting has recently provided very satisfactory results to discern between eccentricities and misalignments, among other benefits [8], [18]. The idea of the transient analysis is well-known and relies on identifying the time-frequency evolutions of characteristic fault components under starting. These evolutions yield particular patterns that are reliable evidence of the presence of the fault, since they are unlikely caused by other faults or phenomena [17]. In the current version of the collaborative system, it enables to diagnose rotor damages and eccentricities/misalignments. This latter can be done by combining current and stray flux information [19]. Table I shows the main components amplified by these faults at steady-state that are considered by the intelligent system (*f*=supply frequency, *s*=slip f_r=rotational frequency and *p*= pole pairs). Additionally, Fig. 1 shows the characteristic evolutions of these components under starting (considering *p*=2). The detection of which is the basis of the transient module of the proposed system.

TABLE I. MAIN FREQUENCY COMPONENTS AMPLIFIED BY DIFFERENT FAULTS AT STEADY-STATE

CURRENT	
Rotor faults	$f\cdot(1\pm2\cdot s)$
Eccentricities/misalignments	$f_{ecc}=f\cdot\pm f_r$
STRAY FLUX	
Rotor faults	$s\cdot f$, $3\cdot s\cdot f$ (axial) $f\cdot(1\pm2\cdot s)$ (radial)
Eccentricities	$f_{ecc}= f\cdot\pm f_r$

As shown in Fig.1, there are some components which are associated with rotor faults and others with eccentricities/misalignments. These components have different nature (axial/radial) and may be visible either in the starting current analysis, and in the stray-flux analysis under starting or in both of them, as stated in previous works [8], [18].

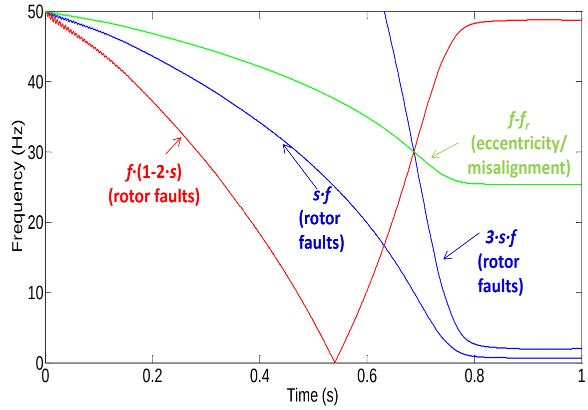

Figure 1. Expected evolutions of the fault harmonics under starting.

To identify and characterize such evolutions, in this paper it is introduced an indicator, which is equivalent to the arithmetic mean for the peak energy values found in a specific time-frequency (t-f) region (R) of the STFT t-f maps. This indicator is given by (1).

$$\overline{R} = \frac{1}{t_f - t_i}\left(\sum_{i=t_i}^{t_f} \gamma_R(i)\right) \tag{1}$$

where $\gamma_R(i)$, which is given by (2), is the peak value at time sample i of the t-f map enclosed region R, and t_i and t_f are, respectively, the initial and final time samples defining the considered t-f area.

$$\gamma_R(i) = Max(E_{i,j})_{j=f_i \dots f_f} \tag{2}$$

where $E_{i,j}$ is the normalized (over the fundamental component) energy density at the (i, j) coordinate of the time-frequency map, and f_i and f_f are, respectively, the initial and final frequency samples defining the considered t-f region R. In order to achieve an automated final diagnosis, it is proposed to use a FFNN with hyperbolic tangent sigmoid and linear activation functions in the hidden and output layers, respectively. This architecture allows for an easy learning generalizing its suitability about the data with which it is trained [20]. Furthermore, this model is selected due to its simplicity, low computational burden, and high performance as an automatic classifier.

III. Proposed Diagnostic Methodology

The proposed methodology for the automatic diagnostic of broken rotor bars and/or eccentricities/misalignments in induction motors by analyzing stray flux and current signals is shown in Fig. 2. It is based on the tracking of the power density at specific regions of interest which are penetrated by the different fault components during their evolutions under the startup transient as follows:

1) Acquire the different stray flux component signals by means of an appropriate DAS (data acquisition system) module during the starting transient namely: radial stray flux (ϕ_1), axial stray flux (ϕ_2), and stator current (C_1). The method requires a minimum length for the startup in order to identify the characteristic pattern associated with the studied faults; as a guideline, with starting times above 0.5 s, the method is suitable.
2) Apply a suitable time-frequency decomposition mathematical tool in order to get a map containing the time-frequency (t-f) information of the acquired signals. For the purposes of this work, it is used the STFT due to its simplicity and wide availability in diverse mathematical software packages.
3) Using (1), compute the indicator $\bar{R}$ for the different regions of interest: R1R, R2R, …, R4C (see Fig. 2). These regions match to specific zones where the characteristic fault components evolve during starting, and to specific regions where harmonics of interests prevails at steady state. Region 1 (R1R, R1A, and R1C) cover the complete starting transient, and the other regions expanse during at least 1 s in time at steady-state. A 1 s time length is recommended as minimum size in order to capture short-time transient states and avoid processing noise produced by external sources. The automation process used to isolate the starting transient consist in obtaining the upper envelope of the time signal, and then setting a threshold value equal to the upper envelope amplitude at steady state (which can be obtained from the last samples).
4) Classify the level of damage: healthy motor (HLT), 2 broken rotor bars (2 BRB), 1 broken rotor bar (1 BRB), and misalignment (MAL) by evaluating the different region indicators. For the purposes of this paper, it is used a FFNN having two hidden layers with 2 and 8 neurons in each hidden layer, respectively.
5) Provide a final diagnosis to the end user through a user interface. In this paper, the use of a touch screen is proposed due to its ease of use, high capacity to display information, and very low cost.

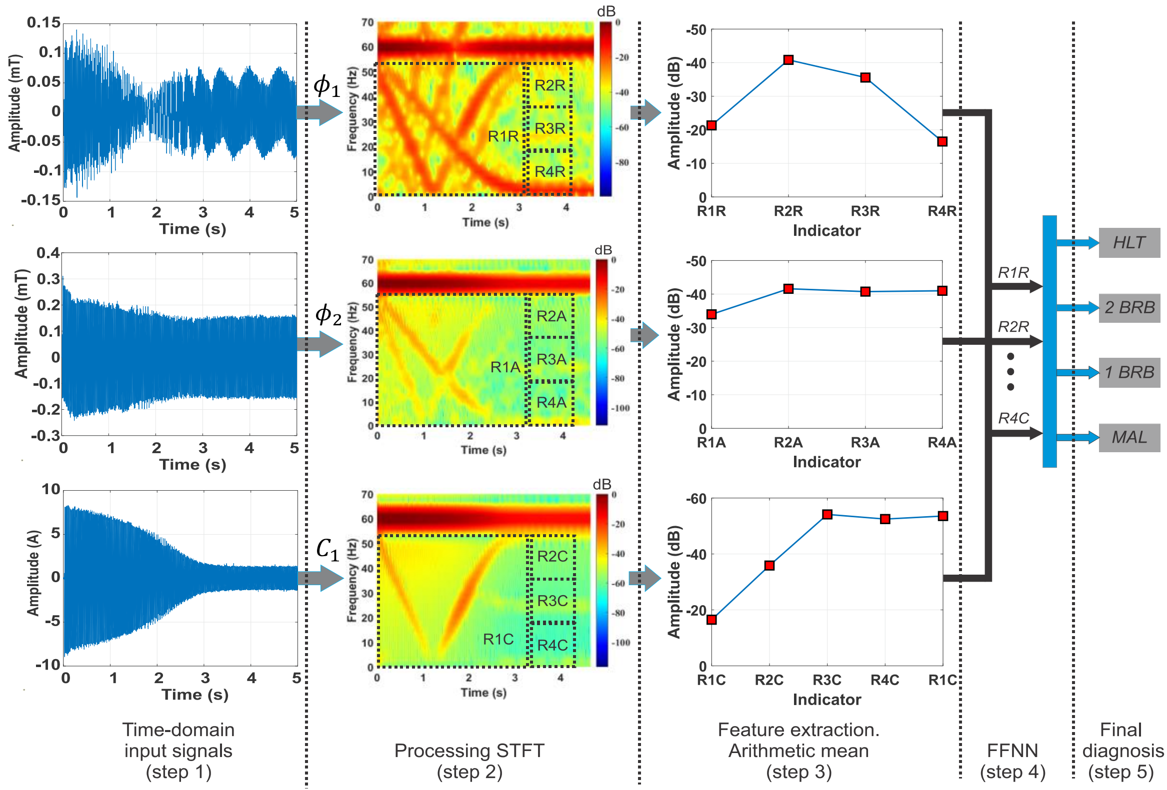

Figure 2. Proposed methodology flow-up.

IV. Smart Sensor Structure

The smart sensor is developed based on the methodology shown in Fig. 2 by following the five steps described there. In this way, in step 1 the stray flux and current data acquisition is achieved by means of a proprietary DAS module based on a signal conditioning stage and a Texas Instrument microcontroller model MSP432P401R, which includes an analog to digital converter (ADC) with 14-bit precision. The main triaxial stray flux sensor is essentially made up by the combination of three individual Hall-effect primary sensors as the one depicted in Fig. 3(a). Each of the primary sensors are ALLEGRO ™ microsystems brand, model A1325 having a sensitivity of 5mV/G. This sensor is 3.02 mm wide by 4.1 mm high, and it has an output voltage proportional to the magnetic flux density as indicated by the manufacturer in their respective datasheet. The primary sensors are located on perpendicular axis to each other in order to capture the axial and radial stray flux components regardless of their relative location to the motor frame. Figure 3 (a) shows a schematic picture of this triaxial stray flux sensor. Each sub-sensor enables the capture of a certain portion of the flux: whereas sub-sensor 1 mainly captures the axial flux, sub-sensor 3 captures the radial one. Sub-sensor 2 captures a combination of both, if installed on the frame of the machine as in Fig. 3(b). Note that this sensor may be easily by a common metal (e.g., copper, steel, aluminum) in order to reject some electromagnetic interference (EMI) encountered on any harsh environment. Therefore, plenty of information is obtained for the diagnosis, since both axial and radial fault components can be identified in the resulting analyses. With regards to current data acquisition, the sensor has an additional input channel connected to a current clamp that enables to capture the current signals. Figure 3 (b) shows the proposed triaxial stray flux sensor installed on the frame of an induction motor. This sensor has the flexibility to be installed in almost any place on the frame of electric machines since it is a very small size sensor.

The smart-sensor processing unit, which performs steps 2 to 4 is based on a raspberry pi model 3 that has a 4 × ARM Cortex-A53 processor. Firstly, the processing unit performs the STFT to the starting and steady-state signals by using the parameters detailed in [21]. Then, steps 3 and 4 are carried out internally by computing the proposed indicators (R1R, R2R, …, R4C), and then feeding them to a previously trained FFNN. This procedure allows for the discrimination between the studied faults by analyzing and comparing the stray flux and current signals [19]. If the rotational frequency component appears only in the current analyses, they are likely due to the misalignment whereas if it appears in both analyses, they are probably due to eccentricity problems, as reported in [19].

In order to provide an in-situ final diagnosis and show the results to the final user, a raspberry touchscreen is used. The user interface (shown in Fig. 3(c)) is composed mainly by three sections: stray flux / current spectrogram selection, which selects the spectrogram to be visualized by the end-user, start-up transient spectrogram visualization region, which shows a t-f map of the selected signal, and a quantified final diagnosis, which shows an automated final diagnosis by selecting between the different faults studied in this paper. Finally, the smart sensor is able to store and share any collected data to a PC via a USB interface.

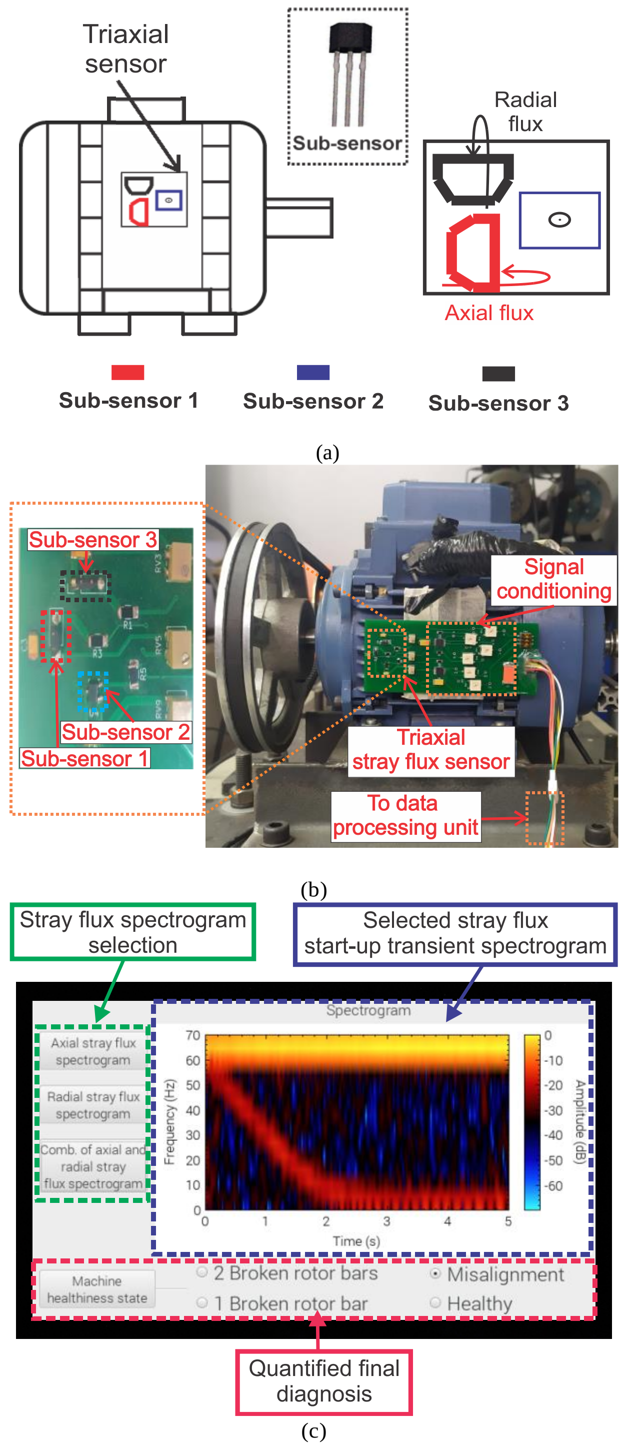

Figure 3. smart sensor general structure; (a) schematic triaxial stray flux sensor view; (b) triaxial stray flux sensor and signal conditioning stage; (c) in-situ final diagnosis and user interface touchscreen.

V. EXPERIMENTAL SETUP

Several tests were carried out in order to assess the validity of the smart sensor under a variety of operating conditions, namely: healthy motor (HLT), healthy motor with misalignment in the coupling system (MAL), 1 broken rotor bar (1 BRB), and 2 broken rotor bars (2 BRB). Moreover, two different induction motors having distinct constructive characteristic were analyzed as different study cases, namely: on the hand, a WEG 00136APE48T 2-pole, 1 HP, 220 V cage induction motor with 28 bars that was coupled to an alternator by means of a belts and pulleys system (see Fig. 4(a)). This mechanical load represents 25% of rated load for the motor. On the other hand, a SIEMENS 4-pole, 400-V, 1.47 HP cage induction motor with 28 bars. To produce an artificial broken rotor bar condition, a 2.0 mm diameter hole was drilled in one and two bars of the rotor without harming the rotor shaft as shown in Fig. 4(b). Then, in order to force misalignment faults, the band in the motor pulley was shifted forward, so that the transverse axes of rotation for the motor and its load were not aligned forming a gap angle β as shown in Fig. 4(c). This condition can be clearly seen by comparing the aligned motor (Fig. 4(d)) and the misaligned motor (Fig. 4(c)). The stray flux and current signals are captured and stored using a proprietary DAS module based on a 14-bit resolution Texas Instrument analog-to-digital converter at a sampling frequency $f_s = 5\,kHz$. The induction motor is driven under a direct-online start.

The FFNN is trained through the Levenberg-Marquardt algorithm for identifying a healthy induction motor, 1 BRB fault, 2 BRB fault, and MAL fault. For this, a total of 160 signals were captured and extracted from the measurement during the starting transient and 1 s after starting transient (40 per fault condition state). From the 160 signals obtained, 80 are used for the training of the FFNN and 80 for validation. The FFNN final architecture has 12 inputs ($R1R, R2R, \dots R4C$), 2 and 8 neurons in the hidden layers, and 4 outputs (one per each fault condition studied here). The number of 4 and 8 neurons in the hidden layer is selected by trial and error in order to obtain the minimum overall classification error, as suggested in [22].

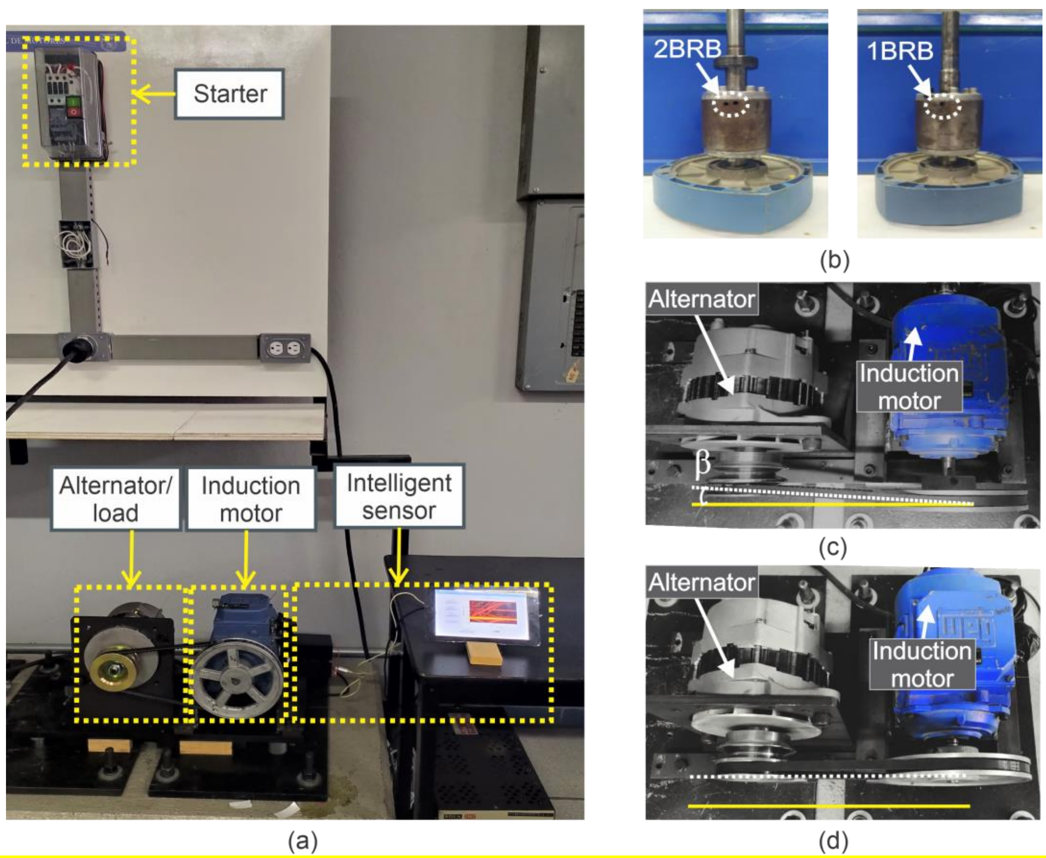

Figure 4. Experimental setup: (a) laboratory testbench; (b) broken rotor bars; (c) motor aligned with load; (d) motor misaligned with load.

VI. TESTS AND RESULTS

The analyzes and results shown in this section are performed by the smart sensor itself; however, some of the figures have been edited (using the stored data from the smart sensor) in order to give a better presentation of the results of this work. Figure 5 shows the internal STFT analyses of the stray flux signals captured by each sub-sensor for different fault conditions. Note the presence of the evolutions of the fault components predicted by the theory and depicted in Fig. 1: on the one hand, the axial component at $s{\cdot}f$ is clearly visible (especially, at sub-sensor 1 and 2, which mainly capture the axial flux), while the evolution of the radial component $f{\cdot}(1\text{-}2{\cdot}s)$

is especially visible at sub-sensor 3, which mainly captures the radial stray flux. Note that the identification of the evolutions of multiple components linked with the failure (in this case, the axial and radial ones), by using several sub-sensors, enables to reach a more reliable diagnosis.

On the other hand, Fig. 8 shows the STFT analyses of the starting current. The information obtained is less rich in harmonics, but it enables to diagnose the presence of the rotor damage through the presence of the $f\cdot(1\text{-}2\cdot s)$ component evolution. The misalignment caused by the coupling system can be identified through the appearance of the corresponding components in the current analyses (see f_{ecc}, note the pulleys diameter ratio) but not in the stray flux analyses. As commented in [19], if this component appears in the starting current analyses but it does not show up in the stray flux analyses (as it happens in this case), then it is mainly attributed to a misalignment between the motor and the driven load, whereas if it appears in both analyses it is due to eccentricity faults.

Figure 6 shows the peak values tracked in the STFT plot under starting for 2 broken rotor bars, 1 broken bar, and healthy motor with misalignment, and for the different stray fluxes. Note the higher energy density found in the radial stray flux t-f map during the start-up, especially for the case of 2 BRB. A gradualness can be clearly seen when the fault severity increases, that is, the energy density is greater when the motor operates under 2 BRB than 1 BRB. The distribution of the indicator R1R obtained for the 160 tests performed (40 test per each condition state studied here) confirms this situation (see Fig. 7). A distribution with higher R1R values is obtained for more severe broken rotor bar damages. Similar results are obtained by analysing the current signals, as shown in Fig. 9.

On the other hand, Fig. 10 shows the results obtained when analysing the case study 2 (1.47 HP induction motor). Note that the starting transient of this motor is much faster and it lasts approximately 1s. The results shown in this figure demonstrate the capability of the proposal to also diagnose electric motors with startup transients lasting 1s or less, since the normalized proposed indicators remains under closed intervals and amplitudes according to the fault. The smart sensor system has been validated in a wide range of operating conditions (various loading levels and supply voltages), yielding a very high success rate in the determination of its real condition. The objective is to test its validity in wider number of motors with different power ranges and constructive characteristics. Additionally, due to the flexibility of the proposed methodology, the boundaries of the specific regions of interest (i.e., R1R, R2R, …, R4C) can be redefined according to the actual trajectories followed by the fault harmonics during the startup transient, which can be modified depending on the motor drive settings.

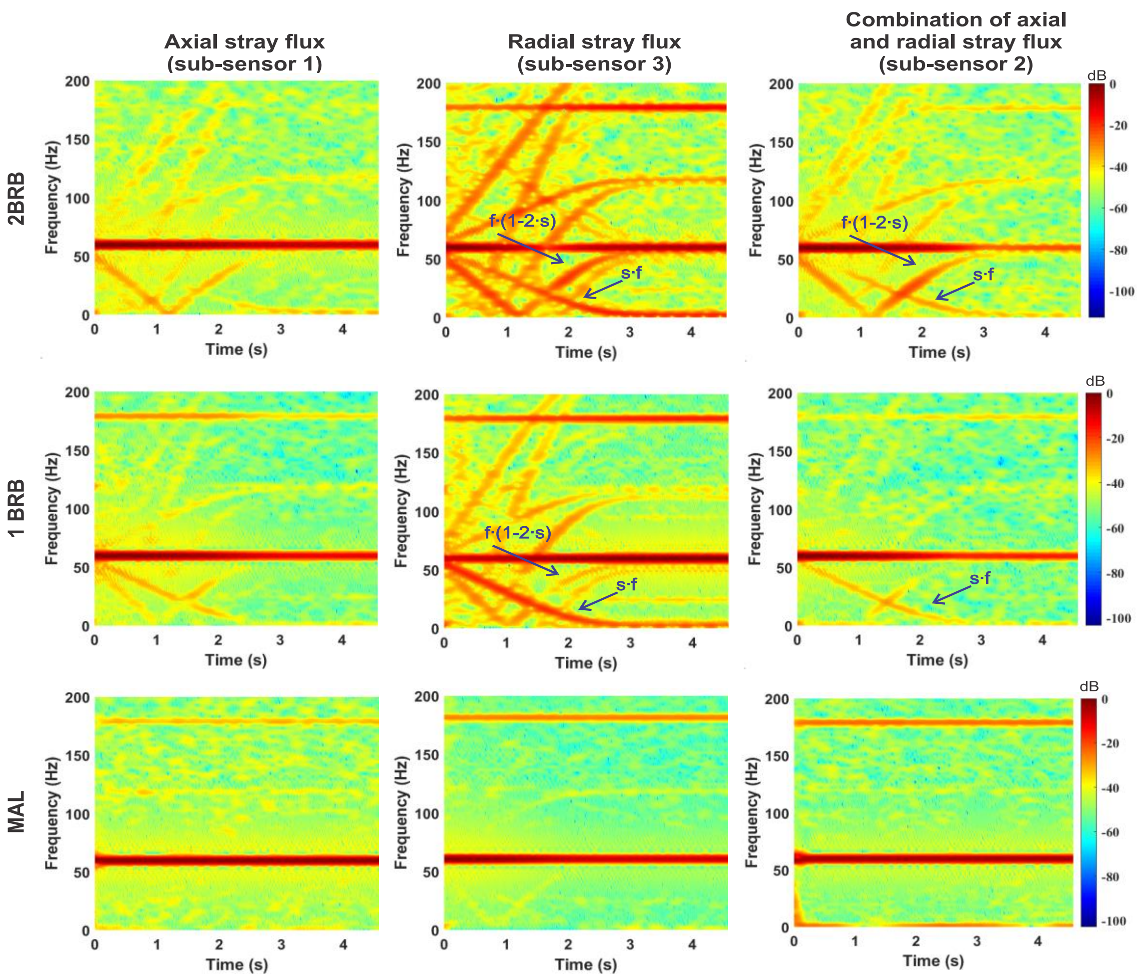

Figure 5. STFT analyses of starting stray-flux signals performed by the smart-sensor for the first case study (1 HP induction motor).

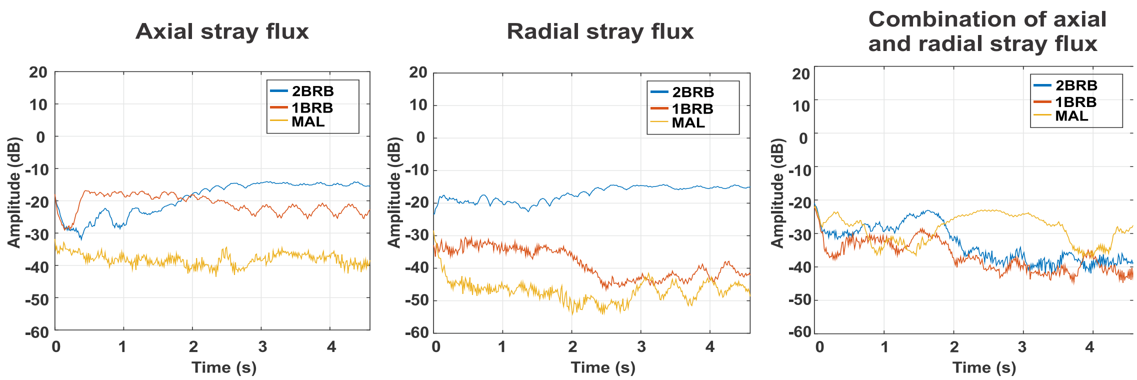

Figure 6. Experimental results for the peak values found in the STFT plot under starting for the first case study (1 HP induction motor) having 2 broken rotor bars, 1 broken bar, and healthy motor with misalignment for the different stray flux signals.

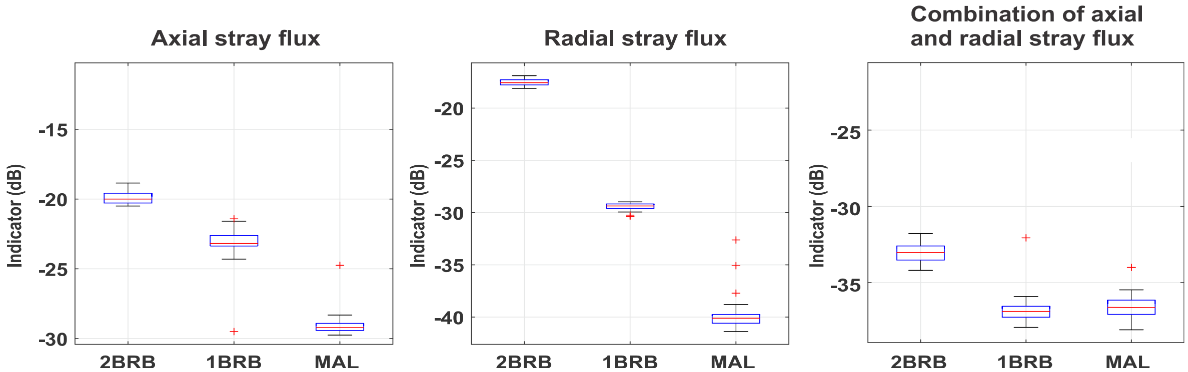

Figure 7. Boxplots obtained from the experimental results of the indicator R1R for the first case study (1 HP induction motor).

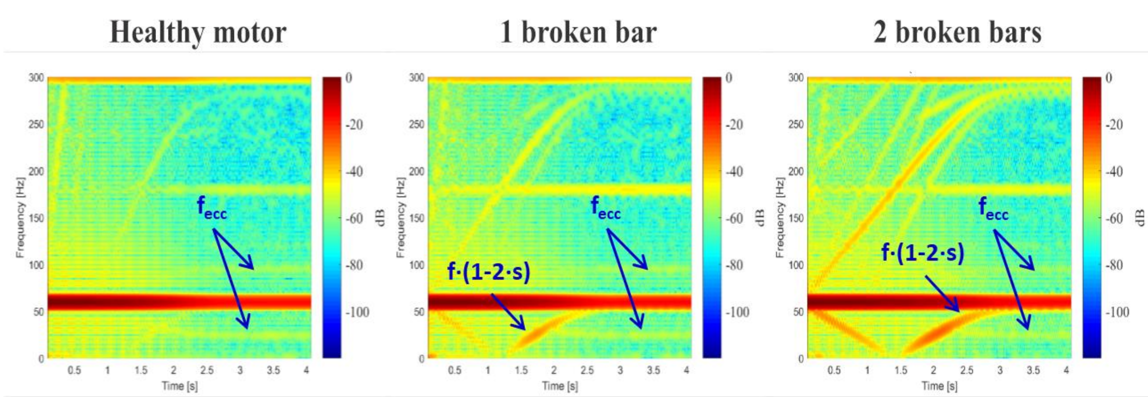

Figure 8. STFT analyses of starting current signal performed by the smart sensor for the first case study (1 HP induction motor).

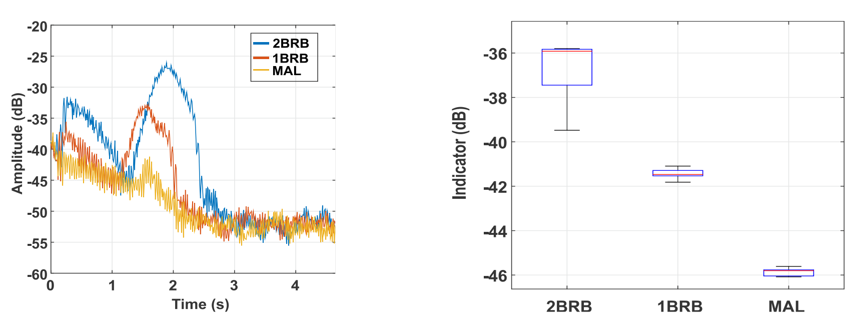

(a) (b)

Figure 9. Experimental results of the proposed method for the first case study (1 HP induction motor): (a) peak values found in the STFT plot under starting for the current signals and the different fault conditions studied here; (b) boxplot of the R1C indicator obtained from the tests performed.

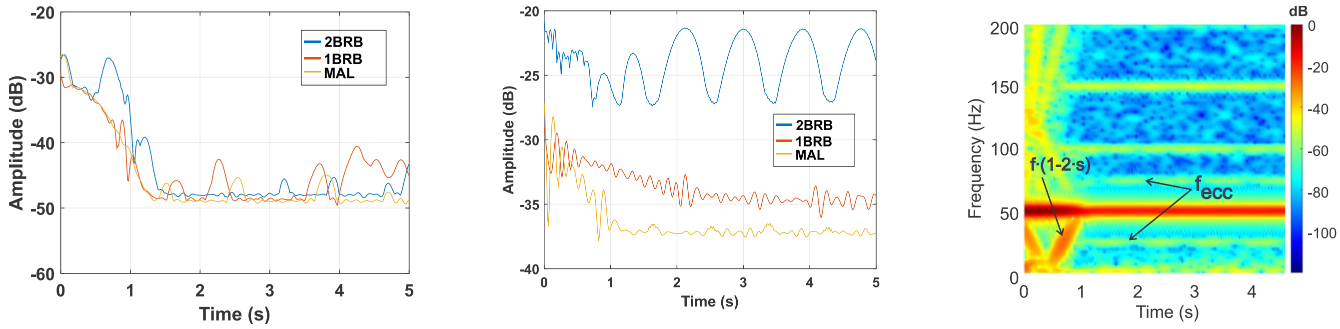

(a) (b) (c)

Figure 10. Experimental results of the proposed method for the second case study (1.47 HP induction motor): (a) peak values found in the STFT plot under starting for the current signals; (b) peak values found in the STFT plot under starting for the radial stray flux signals; (c) STFT analyses of starting stray-flux signals.

Table II shows the classification results as well as the effectiveness percentage of the proposed methodology. Correct classifications are located in the diagonal of Table II (highlighted in bold). Through the proposed methodology it is possible to correctly classify the faults studied here with an effectiveness of 95% (worst case, which occurs in the case of small misalignment). The effectiveness, per fault studied, is obtained through the calculation of the fault detection rate index (FDR) by dividing the number of correct classifications over the total number of samples

TABLE II. EFFECTIVENESS PERCENTAGE OF THE PROPOSED METHODOLOGY (CONFUSION MATRIX).

	2 BRB	1 BRB	MAL	HEALTHY	Effectiveness (%)
2 BRB	**20**	0	0	0	100
1 BRB	0	**20**	0	0	100
MAL	0	0	**19**	1	95
HEALTHY	0	0	0	**20**	100

VII. CONCLUSIONS

This paper presents a novel smart sensor based on the advanced analysis of stray flux and current data for the diagnosis of failures in induction motors. Unlike other solutions, the underlying processing unit relies on the analysis of both quantities under stationary and transient conditions. This feature provides a much higher reliability for the diagnosis. The hierarchical structure of the internal decision system, based on a feed forward neural network, enables to combine the diagnostic provided by both quantities, in such a way that it is possible to discern between different types of mechanical faults (e.g. eccentricities and misalignments). This feature provides the smart-sensor with a great flexibility to achieve automated final diagnosis about different electromechanical faults. As shown in the results, the peaks of the energy found in the t-f maps during starting and steady state provide relevant information related to broken rotor bars and misalignment faults. Furthermore, the combined analysis of stray flux and current signals performed by the smart-sensor provides a robust and in-situ final diagnosis.

The proposed method requires a minimum startup transient length in order to identify the different patterns associated with each fault. As a guideline, the method is suitable to be applied under a minimum startup transient of 0.5 s, which represents the great majority of machines on the industry. Moreover, at this stage, the method is suited for line-fed operation, but it can be adapted to inverter-fed motors, considering that the evolutions of fault components are different [23].

The sensor is planned to be applied to the detection of additional faults and, also, it is designed to incorporate other valuable inputs (e.g. infrared data). Moreover, more fault scenarios are possible to be diagnosed; however, a redefinition of the boundaries of the regions of interest may be required as well as retraining of the FFNN according to the characteristic pattern yielded by the fault evolution of interest. This redefinition implies that the fault to be diagnosed is clearly visible in the t-f map of either current signals or stray flux signals.

ACKNOWLEDGMENT

We would like to thank Consejo Nacional de Ciencia y Tecnología (CONACYT Scholarship with key code 2019-000037-02NACF).

REFERENCES

[1] W. T. Thomson and M. Fenger, “William T. Thomson and Mark Fenger,” IEEE Ind. Appl. Mag., no. August, 2001.

[2] M. Garcia, P. A. Panagiotou, J. A. Antonino-Daviu, and K. N. Gyftakis, “Efficiency assessment of induction motors operating under different faulty conditions,” IEEE Trans. Ind. Electron., vol. 66, no. 10, pp. 8072–8081, 2019, doi: 10.1109/TIE.2018.2885719.

[3] J. Herrera-Guachamin and J. Antonino-Daviu, “Laboratory experiments for the evaluation of the efficiency of induction motors operating under different electrical and mechanical faults,” IECON Proc. (Industrial Electron. Conf., vol. 2019-October, pp. 6319–6322, 2019, doi: 10.1109/IECON.2019.8927328.

[4] W. R. Finley, M. M. Hodowanec, and W. G. Holter, “Diagnosing motor vibration problems,” IEEE Conf. Rec. Annu. Pulp Pap. Ind. Tech. Conf., pp. 165–180, 2000, doi: 10.1109/papcon.2000.854217.

[5] J. R. Cameron, W. T. Thomson, and A. B. Dow, “Vibration and current monitoring for detecting airgap eccentricity in large induction motors,” IEE Proc. B Electr. Power Appl., vol. 133, no. 3, pp. 155–163, 1986, doi: 10.1049/ip-b.1986.0022.

[6] A. G. Garcia-Ramirez, L. A. Morales-Hernandez, R. A. Osornio-Rios, J. P. Benitez-Rangel, A. Garcia-Perez, and R. D. J. Romero-Troncoso, "Fault detection in induction motors and the impact on the kinematic chain through thermographic analysis," Electric Power Systems Research, vol. 114. pp. 1–9, 2014, doi: 10.1016/j.epsr.2014.03.031.

[7] D. Lopez-Perez and J. Antonino-Daviu, "Application of Infrared Thermography to Failure Detection in Industrial Induction Motors: Case Stories," IEEE Trans. Ind. Appl., vol. 53, no. 3, pp. 1901–1908, 2017, doi: 10.1109/TIA.2017.2655008.

[8] J. A. Ramirez-Nunez et al., "Evaluation of the Detectability of Electromechanical Faults in Induction Motors Via Transient Analysis of the Stray Flux," IEEE Trans. Ind. Appl., vol. 54, no. 5, pp. 4324–4332, 2018, doi: 10.1109/TIA.2018.2843371.

[9] B. Y. G. C. Stone, M. K. W. Stranges, D. G. Dunn, T. Ieee, and I. E. Com-, "Common Questions on Partial Discharge Testing," IEEE Ind. Appl. Mag., no. Jan/Feb 2016, pp. 14–19.

[10] G. C. Stone, H. G. Sedding, and C. Chan, "Experience with Online Partial-Discharge Measurement in High-Voltage Inverter-Fed Motors," IEEE Trans. Ind. Appl., vol. 54, no. 1, pp. 866–872, 2018, doi: 10.1109/TIA.2017.2740280.

[11] A. Glowacz, "Fault diagnosis of single-phase induction motor based on acoustic signals," Mech. Syst. Signal Process., vol. 117, pp. 65–80, 2019, doi: 10.1016/j.ymssp.2018.07.044.

[12] M. Riera-Guasp, J. A. Antonino-Daviu, and G. A. Capolino, "Advances in electrical machine, power electronic, and drive condition monitoring and fault detection: State of the art," IEEE Trans. Ind. Electron., vol. 62, no. 3, pp. 1746–1759, 2015, doi: 10.1109/TIE.2014.2375853.

[13] S. Lu, G. Qian, Q. He, F. Liu, Y. Liu, and Q. Wang, "In Situ Motor Fault Diagnosis Using Enhanced Convolutional Neural Network in an Embedded System," IEEE Sens. J., vol. 20, no. 15, pp. 8287–8296, 2020, doi: 10.1109/JSEN.2019.2911299.

[14] I. Zamudio-Ramirez, R. A. Osornio-Rios, and J. Antonino-Daviu, "Triaxial Smart Sensor Based on the Advanced Analysis of Stray Flux and Currents for the Reliable Fault Detection in Induction Motors," ECCE 2020 - IEEE Energy Convers. Congr. Expo., pp. 4480–4484, 2020, doi: 10.1109/ECCE44975.2020.9235938.

[15] I. Zamudio-Ramírez, R. A. Osornio-Ríos, J. A. Antonino-Daviu, and A. Quijano-Lopez, "Smart-sensor for the automatic detection of electromechanical faults in induction motors based on the transient stray flux analysis," Sensors (Switzerland), vol. 20, no. 5, 2020, doi: 10.3390/s20051477.

[16] I. Zamudio-Ramirez, R. A. Osornio-Rios, M. Trejo-Hernandez, R. De Jesus Romero-Troncoso, and J. A. Antonino-Daviu, "Smart-Sensors to Estimate Insulation Health in Induction Motors via Analysis of Stray Flux," Energies, vol. 12, no. 9, pp. 1–16, 2019, doi: 10.3390/en12091658.

[17] J. A. Antonino-Daviu, J. Pons-Llinares, and S. Bin Lee, "Advanced rotor fault diagnosis for medium-voltage induction motors via continuous transforms," IEEE Trans. Ind. Appl., vol. 52, no. 5, pp. 4503–4509, 2016, doi: 10.1109/TIA.2016.2582720.

[18] I. Zamudio-Ramirez, J. A. Antonino-Daviu, R. A. Osornio-Rios, R. De Jesus Romero-Troncoso, and H. Razik, "Detection of Winding Asymmetries in Wound-Rotor Induction Motors via Transient Analysis of the External Magnetic Field," IEEE Trans. Ind. Electron., vol. 67, no. 6, pp. 5050–5059, 2020, doi: 10.1109/TIE.2019.2931274.

[19] Y. Park, H. Choi, J. Shin, J. Park, S. Bin Lee, and H. Jo, "Airgap flux based detection and classification of induction motor rotor and load defects during the starting transient," IEEE Trans. Ind. Electron., vol. 67, no. 12, pp. 10075–10084, 2020, doi: 10.1109/TIE.2019.2962470.

[20] J. Feng and S. Lu, "Performance analysis of various activation functions in artificial neural networks," in Journal of Physics: Conference Series, 2019, vol. 1237, no. 2, p. 22030.

[21] J. Pons-Llinares, M. Riera-Guasp, J. A. Antonino-Daviu, and T. G. Habetler, "Pursuing optimal electric machines transient diagnosis: The adaptive slope transform," Mech. Syst. Signal Process., vol. 80, pp. 553–569, 2016, doi: 10.1016/j.ymssp.2016.05.003.

[22] D. Camarena-Martinez, M. Valtierra-Rodriguez, A. Garcia-Perez, R. A. Osornio-Rios, and R. D. J. Romero-Troncoso, "Empirical mode decomposition and neural networks on FPGA for fault diagnosis in induction motors," Sci. World J., vol. 2014, p. 908140, 2014, doi: 10.1155/2014/908140.

[23] J. Pons Llinares; D. Morinigo-Sotelo; O. Duque-Perez; J. Antonino-Daviu; M. Pérez Alonso (2014). Transient Detection of Close Components through the Chirplet Transform: Rotor Faults in Inverter-Fed Induction Motors. *40th Annual Conference of the IEEE Industrial Electronics Society* (IECON 2014). (3386 - 3392). Dallas, USA.

BIOGRAPHIES

Israel Zamudio-Ramírez received his M.S. degree in mechatronic from the Autonomous University of Queretaro, Mexico, in 2019. He is currently working towards the Ph.D. degree at the Autonomous University of Queretaro with the Department of Mechatronics, Mexico and at the Universitat Politècnica de València with the Department of Electrical Engineering, Spain. His research interests include monitoring and diagnosis of electrical machines, embedded systems and hardware signal processing for engineering applications on FPGA.

Roque Alfredo Osornio-Rios (Member, IEEE) received the Ph.D. degree in mechatronics from the Autonomous University of Queretaro, Queretaro, Mexico, in 2007. He is a National Researcher level 3 with the Mexican Council of Science and Technology, CONACYT. He is currently a Head Professor with the Department of Mechatronics, University of Queretaro. He is an Advisor for more than 80 theses, and has coauthored more than 100 technical papers published in international journals and conferences. His research interests include hardware signal processing and mechatronics. Dr. Osornio-Rios is a Fellow of the Mexican Academy of Engineering. He is part of the editorial board of Journal and Scientific and Industrial Research.

Jose Antonino-Daviu (S'04, M'08, SM'12) received his M.S. and Ph. D. degrees in Electrical Engineering, both from the Universitat Politècnica de València, in 2000 and 2006, respectively. He also received his Bs. in Business Administration from Universitat de Valencia in 2012. He was working for IBM during 2 years, being involved in several international projects. Currently, he is Full Professor in the Department of Electrical Engineering of the mentioned University, where he develops his docent and research work. He has been invited professor in Helsinki University of Technology (Finland) in 2005 and 2007, Michigan State University (USA) in 2010, Korea University (Korea) in 2014 and Université Claude Bernard Lyon 1 (France) in 2015. He is IEEE Senior Member since 2012 and he has published over 200 contributions, including international journals, conferences and books. He is also Associate Editor of IEEE transactions on Industrial Informatics and IEEE Industrial Electronics Magazine and he is also IEEE IAS Distinguished Lecturer for 2019-20. He was General Co-Chair of IEEE SDEMPED 2013. He received the Nagamori Award from Nagamori Fundation in Kyoto, Japan in 2018, for his contributions in electric motors transient analysis area. In 2019, he was awarded with the SDEMPED Diagnostic Achievement Award in Toulouse, France.